Quantum Mechanical/Molecular Mechanical Molecular Dynamics Simulations of Cytidine Deaminase: From Stabilization of Transition State Analogues to Catalytic Mechanisms

Qin Xu and Hong Guo*

Department of Biochemistry and Cellular and Molecular Biology, Center of Excellence in Structural Biology, University of Tennessee, Knoxville, Tennessee 37996-0840

Received: November 19, 2003

Cytidine deaminase catalyzes the hydrolytic deamination of cytidine to uridine and accelerates the rate of the reaction by 10^{11}-fold. The enzyme is strongly inhibited by the transition state analogue inhibitor zebularine 3,4-hydrate, and a fraction of transition state stabilization is captured by the interaction of this inhibitor at the active site. QM/MM molecular dynamics and free energy simulations are performed for *Escherichia coli* cytidine deaminase (CDA) complexed with zebularine 3,4-hydrate to understand the origin of the structural stability of zebularine 3,4-hydrate in the active site and elucidate the mechanism of the CDA-catalyzed reaction. It is shown that the existence of Glu-104 is essential for the structural stability and integrity of zebularine 3,4-hydrate. The simulations also reveal that the covalent bond between C_4 and the 4-OH group in ZEB−H_2O undergoes transient bond-breaking and -making in the active site, resembling the process of the nucleophilic attack by the zinc hydroxide group on C_4 during the catalysis. The role of the active-site interactions in stabilizing zebularine 3,4-hydrate and transition state is discussed. The results demonstrate that understanding the stability and integrity of TSA's in the active sites may provide important insights into the origin of transition state stabilization.

Introduction

Enzymes are the most proficient catalysts. Their catalytic power lies in the enzyme's ability to stabilize transition state (TS) and to lower the energy barriers for enzyme-catalyzed reactions, although other factors may be involved as well. Understanding the forces responsible for transition state stabilization is of fundamental importance for a microscopic description of the catalytic mechanism, but also for the design of effective enzyme inhibitors or improvement of existing enzymes (or abzymes) for catalyzing chemical reactions. It has been recognized[1−3] that a molecule that mimics the altered structure of substrate in the transition state should bind to the enzyme tightly, and such a transition state analogue (TSA) may capture a significant fraction of transition state stabilization. The enzyme−TSA complexes, where the inhibitors are designed on the basis of possible catalytic mechanisms, can therefore be used as models for understanding the properties and structural features of transition states (which have a very short lifetime and are difficult to study). A number of the TSA inhibitors have been identified.[4−8] It has been shown that some of them can indeed bind to enzymes significantly stronger than the corresponding substrates, as originally hypothesized.[1] The precise arrangements of many TSA inhibitors in the enzyme active sites have also been determined by X-ray crystallography,[9,10] which led to significant insights into the structural origins of enzyme catalysis as well as the possible roles of active-site interactions in transition state stabilization.

The ability of well-designed TSA's to mimic the transition state or intermediate structures and to capture a significant fraction of transition state affinity implies that the structural stability and integrity of TSA's in the active sites may depend, at least in some of the cases, on the same forces that are responsible for transition state stabilization during the enzyme-catalyzed reactions. Removal of certain key residues crucial for the stability and integrity of the TSA inhibitors could also affect the transition state stabilization and lead to a reduced catalytic efficiency. Thus, determination of the conditions for existence of stable TSA's in the enzyme active sites should be of considerable interest, as the problem of understanding the origin of transition state stabilization might be simplified to a stability problem concerning TSA's in the enzyme's active sites. The large number of high-resolution structures of enzyme−TSA complexes[9,10] can be used directly as the initial coordinates in computational studies; they may also serve as an important testing ground for theoretical predictions. Although all the questions concerning transition state stabilization and catalytic mechanisms are unlikely to be solved on the basis of our understanding of the stability of TSAs in the active sites alone, important insights may be obtained from such studies.

Here quantum mechanical/molecular mechanical (QM/MM) molecular dynamics simulations are performed for *Escherichia coli* cytidine deaminase (CDA)[11] complexed with the transition state analogue zebularine 3,4-hydrate (ZEB−H_2O) (Figure 1B) to elucidate the origin of the stabilization of zebularine 3,4-hydrate by the active-site interactions. One advantage of the QM/MM treatments of the enzyme complex is that they allow the QM part of the system (e.g., ZEB−H_2O and zinc in this study) to undergo chemical transformations during molecular dynamics (MD) simulations in the search for stable chemical structure(s) under a given environment. The free energy approach can be used to determine the free energy changes associated with chemical and conformational transformations. However, it is extremely time-consuming to perform free energy calculations with *ab initio* methods, and semiempirical approaches need to be used. There are different semiempirical methods available. In this paper, we use a semiempirical density functional method, SCC-DFTB,[25a] to describe the QM part,

* Corresponding author.

10.1021/jp037529d CCC: $27.50
Published on Web 01/24/2004

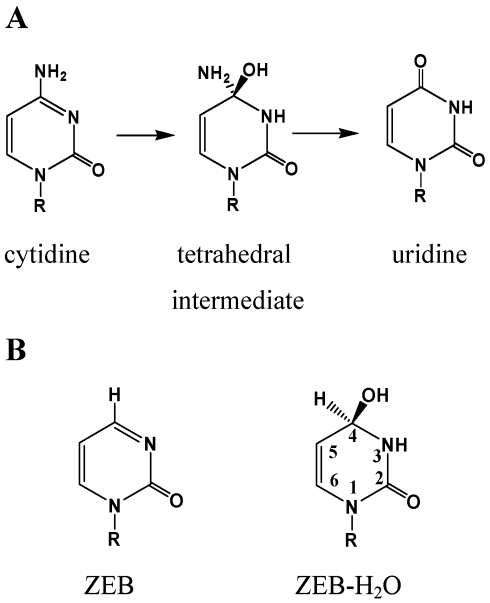

Figure 1. (A) Hydrolytic deamination of cytidine to uridine catalyzed cytidine deaminase via a tetrahedral intermediate. (B) Pyrimidin-2-one ribonucleoside (zebularine or ZEB) and zebularine 3,4-hydrate (ZEB−H_2O). ZEB−H_2O resembles the tetrahedral intermediate in (A), and the hydration process seems to be catalyzed by CDA by a mechanism similar to the formation of the tetrahedral intermediate during the CDA-catalyzed reaction.

because this approach has been extensively tested against high level quantum mechanical methods for a range of active site models containing zinc.[25b] It was found that the SCC-DFTB approach reproduced structural and energetic properties rather reliably for the active sites of these enzymes.[25b] The SCC-DFTB/MM approach has been tested previously for chorismate and used to study the enzyme chorismate mutase.[28,29]

CDA catalyzes the hydrolytic deamination of cytidine to uridine (Figure 1A) and has been a subject of extensive investigations.[11−24] It is one of the more efficient enzymes known with a rate acceleration of 10^{11}-fold.[22] It has been shown that the deamination proceeds stepwise through a tetrahedral intermediate (formed by the nucleophilic attack by the zinc hydroxide group on C_4) with ammonia elimination as the major rate-determining step.[24] The catalysis depends critically on the presence of Glu-104, and the mutation of Glu-104 to Ala reduces k_{cat} by 10^8-fold.[14] The side chain of Glu-104 seems to play multiple roles and is thought to provide all the necessary proton-transfer functions during the catalysis (i.e., generating the zinc hydroxide nuecleophile, protonating the pyrimidine ring nitrogen and shuttling the proton from the 4-OH group to leaving amino group).[12] Glu-104 is believed to be important for transition state stabilization, probably, through the formation of a strong hydrogen bond with the 4-OH group of the tetrahedral intermediate.[11] The observation that the mutation of Glu-104 to Ala increases the enzyme's affinities toward substrate cytidine and product uridine by factors of 30 and 120, respectively, has led to the suggestion that Glu-104 may be involved in the ground state destabilization as well.[13]

Zebularine (ZEB; see Figure 1B) and 5-fluorozebularine (FZEB) bind CDA in hydrated forms (ZEB−H_2O and FZEB−H_2O, respectively),[11,12] and the hydration processes seem to be catalyzed by CDA by a mechanism similar to the formation of the tetrahedral intermediate during the CDA-catalyzed reaction.[10] Interestingly, the ^{19}F NMR resonance[13] of 5-[^{19}F]FZEB showed that whereas the inhibitor is bound by wild-type enzyme as the 3,4-hydrated species, it is bound by the E104A mutant without modification in a form that resembles the substrate in the ground state. The detailed structural origin for the different behavior is still not clear. CDA is strongly inhibited by ZEB−H_2O and FZEB−H_2O; e.g., the enzyme's affinity ($K_i = 1.2 \times 10^{-12}$ M) for ZEB− H_2O exceeds the affinity for the product uridine and the inhibitor 3,4-dihydrozebularine (DHZ) (for which the 4-OH group of ZEB−H_2O is replaced by a hydrogen atom) by a factor of approximately 10^8.[23] Thus, the enzyme appears to have a very strong ability to stabilize the rare 3,4-hydrated species in the active site that resemble the tetrahedral intermediate formed by the nucleophilic attack by the zinc hydroxide group on C_4.[12] In this paper, the stability of ZEB−H_2O is studied, and it is shown that the presence of Glu-104 is essential for the existence of zebularine 3,4-hydrate in the CDA active site. The QM/MM molecular dynamics simulations demonstrate that whereas the covalent bond between C_4 and the 4-OH group in ZEB−H_2O exists in wild-type CDA, it is broken in the E104A mutant followed by a proton transfer from the 3-NH group to the hydroxide. The simulations also show that, unlike conventional covalent bonds, the bond between C_4 and the 4-OH group in the wild-type CDA−ZEB−H_2O complex undergoes large fluctuations and breaks transiently during the simulations. The QM/MM MD simulations of the CDA−ZEB−H_2O complex seem to be able to not only capture the structural features of the CDA−ZEB−H_2O complex but also provide some important insights into the dynamic events associated with the nucleophilic attack by the zinc hydroxide group on C_4 during the catalysis.

Methods

A fast semiempirical density-functional approach (SCC-DFTB),[25] recently implemented in the CHARMM program,[27] was used for QM/MM molecular dynamics simulations.[26] The SCC-DFTB approach has been extensively tested against high level quantum mechanical methods for a range of active site models containing zinc.[25b] It was found that the SCC-DFTB approach reproduced structural and energetic properties rather reliably.[25b] The QM (SCC-DFTB)/MM molecular dynamics simulations have been used recently to study the conformational transitions of substrate in chorismate mutase.[28,29] The initial coordinates for the simulations were obtained from the crystal structures of the CDA−TSA complex (1CTU),[11] which have the transition state analogue ZEB−H_2O at the active site. It has been suggested[19] that there might be a trapped water molecule in the CDA−ZEB−H_2O complex occupying the site of the leaving group (−NH_2 group) of the altered substrate in the transition state. Therefore, a water molecule was manually docked into this site. The MD simulations were performed on the CDA−ZEB−H_2O complexes with and without this additional water, and the results are rather similar. ZEB−H_2O and zinc were treated by QM and the rest of the system by MM. To study the effects of the interactions involving Glu-104 on the stability and integrity of ZEB−H_2O, Glu-104 was simply replaced by Ala on the basis of the X-ray structure of the CDA−ZEB−H_2O complex; the structure for the E104A mutant is not available. The all-hydrogen potential function (PARAM22)[30] was used for MM atoms. A modified TIP3P water model[31,32] was employed for the solvent. The stochastic boundary molecular dynamics method[33] was used for the QM/MM MD simulations. The system was separated into a reaction zone and a reservoir region, which was deleted; the reaction zone was further divided into the reaction region and the buffer region. The reference point for partitioning the system was chosen as the N_1 atom of ZEB−H_2O (Figure 1B). The reaction region was a sphere with radius 16 Å, and the buffer region has *R*

equal to 16 Å ≤ R ≤ 18 Å. Inside the reaction region, the atoms were propagated by molecular dynamics, whereas atoms in the buffer region were propagated by Langevin dynamics. The friction constants for the Langevin dynamics were 250 ps^{-1} for the protein atoms and 62 ps^{-1} for the water molecules. A 1 fs time step was used for integration of the equations of motion, and the results of the simulations were saved on every 50 fs. In initiating the runs, 500 steps of minimization using the steepest descent method were performed for the protein and solvent atoms. Then 4000 steps of minimization were performed for the entire stochastic boundary system with the adapted basis Newton Raphson methods. The temperature of the system was gradually increased from 50 to 300 K (30 ps) and equilibrated at 300 K (40 ps). The simulations were performed on the resulting systems involving ZEB−H_2O for several hundred picoseconds to 1 ns. The umbrella sampling method[34] implemented in the CHARMM program along with the weighted histogram analysis method (WHAM)[35] was applied to determine the change of the free energy (potential of mean force) as a function of the distance (from 1.45 to 3.1 Å) between C_4 and O_4 in ZEB−H_2O; harmonic umbrella potentials with a force constant of 100 kcal $(mole)^{-1}$ $(radian)^{-2}$ were used. Twelve windows were used to go from 1.45 to 3.10 Å. The trajectories obtained from the umbrella sampling were used to study how the active site interactions change as functions of the C_4-O_4 distance. That is, for each window in the umbrella sampling, the average distances for the $OE_2\cdots H_3$, $OE_1\cdots H$ (O_4), and $Zn\cdots O_4$ interactions as well as for the C_4-O_4 bond were obtained from the corresponding trajectory. The average distances from different trajectories were then plotted as functions of the C_4-O_4 distance. The umbrella sampling method was also used to determine the relative stability of the structures before and after the dehydration of ZEB−H_2O in E104A; the difference between $r_1(O_4\cdots H_3)$ and $r_2(N_3-H_3)$ was used as the reaction coordinate with a force constant of 100 kcal $(mole)^{-1}$ $(radian)^{-2}$.

Results

ZEB−H_2O in Wild-Type CDA. An important test for the methods of the QM/MM MD simulations is to see if the structures generated from the simulations agree with the structure determined by X-ray crystallography. In Figure 2A, an average active-site structure based on 2000 frames in the trajectory is compared with that of the X-ray structure.[11] As can be seen from Figure 2A, the active site structure of the CDA−ZEB−H_2O complex from the QM/MM simulations is rather close to the X-ray structure,[11] suggesting the computational approaches used in this study are meaningful. In particular, the 4-OH group of ZEB−H_2O is coordinated to the zinc ion and hydrogen bonded to OE_1 of Glu104. The C_4-O_4 bond has an average distance of about 1.6 Å. OE_2 of Glu-104 receives a hydrogen bond from the 3-NH group. The additional ligands to zinc include Cys-129, Cys-132, and His-102. The distances for some of the interactions between the QM (e.g., zinc) and MM atoms (e.g., the atoms from Cys-129, Cys-132 and His-102) seem to be slightly longer than those in the X-ray structure, but the differences are rather small.

The fluctuation of the C_4-O_4 distance of ZEB−H_2O as a function of time is plotted in Figure 2B; the fluctuation of the $C_3'-O_3'$ distance (in the ribose ring) is also given for comparison. Figure 2B shows that the C_4-O_4 bond is essentially intact with an average distance of ∼1.57 Å. This average distance is somewhat longer than the distance for a normal C−O bond (e.g., for the C3′−O3′ bond of ZEB−H_2O, the average distance is about 1.45 Å). A relatively long C_4-O_4 distance (1.6 Å) was also obtained in the X-ray structure refinement of the CDA−ZEB−H_2O complex,[11] even though a restraint of 1.43 Å was imposed for this bond. The result of the QM/MM MD simulations is therefore consistent with the experimental assignment. It is interesting to note that the distance fluctuations for the C_4-O_4 bond are rather large. A striking observation from Figure 2B is that the C_4-O_4 bond undergoes transient bond-breaking and -making on a picosecond scale during the simulations; the bond distance approaches or exceeds 2.0 Å about 2−3% of the times. Figure 2C shows the free energy (potential of mean force) as a function of the C_4-O_4 distance. Consistent with the earlier observation, there is a second minimum near $r(C_4-O_4) = 2.1$ Å, corresponding to the transient structures with the relatively long C_4-O_4 distances. The existence of two minima indicates that there is equilibrium between two different types of the structures for ZEB−H_2O in the active site.

The changes of the OE_2 (Glu-104)$\cdots H_3$ and OE_1 (Glu-104)$\cdots H$ (O_4) hydrogen bond distances as functions of time are shown in Figure 2D. The role of these two hydrogen bonds has been a subject of previous discussions. It was proposed[11−14] that the interactions involving Glu-104 play an important role in the transition state stabilization, probably through the formation of a strong hydrogen bond between the carboxylate and 4-OH groups. As can be seen from Figure 2D, the two hydrogen bonds involving Glu-104 are rather stable during the simulations. The average distance for the $OE_1\cdots H$ (O_4) hydrogen bond (1.6 Å) is shorter than that for the $OE_2\cdots H_3(N_3)$ hydrogen bond (1.75 Å), consistent with the X-ray structure.[11] It would be of interest to study how the interactions between ZEB−H_2O and CDA change as the C_4-O_4 distance decreases, in a process that mimics the nucleophilic attack by the zinc hydroxide group on C_4 during the CDA-catalyzed reaction. In Figure 2E, the average distances for the $OE_2\cdots H_3$, $OE_1\cdots H$ (O_4), and $Zn\cdots O_4$ interactions obtained from the trajectories in the umbrella sampling (see Methods and Figure 2C above) are given as functions of the C_4-O_4 distance. As is evident from Figure 2E, the $OE_1\cdots H$ (O_4) interaction is very sensitive to the C_4-O_4 distance. When the C_4-O_4 bond is broken (e.g., with a distance greater than 2.1 Å), the $OE_1\cdots H(O_4)$ interaction is rather weak with an average distance of >2.2 Å; the 4-OH group is on the top of the carboxylate plane and does not have the angles for favorable hydrogen bonding interactions with Glu104 (not shown). When the C_4-O_4 bond is formed (i.e., with a distance of 1.5−1.7 Å), OE_1 of Glu104 and 4-OH form a strong hydrogen bond with an average hydrogen bond distance of l.5−1.7 Å. The $OE_2\cdots H_3$ hydrogen bond also strengthens with the formation of the C_4-O_4 bond, but the change is much smaller. It is interesting to note from Figure 2E that the distance between O_4 and Zn increases (from 1.81 to 1.95 Å) with the decreasing C_4-O_4 distance (from 2.3 Å to 1.5 Å). The average distance of 1.95 Å between O_4 and Zn is the same as that of the X-ray structure[11] for the CDA−ZEB− H_2O complex, whereas the distance of 1.81 Å is similar to the distance (1.80 Å) in the CDA−DHZ complex.[11] The distances for the interactions of Zn with Cys-129, Cys-132, and His-102 were also examined. It was found that these distances increase by about 0.05 Å with the decrease of the C_4-O_4 distance. These changes are smaller than that for the $Zn-O_4$ distance (0.15 Å), and quantum mechanical description of the enzyme side chains may be necessary to obtain more reliable results to understand the role of a "valence buffer" in the catalysis.[11]

It is believed that the pyrimidine ring nitrogen at position 3 accepts a proton from Glu104 during the hydration of ZEB and the CDA-catalyzed reaction.[12] To see the effect of this proto-

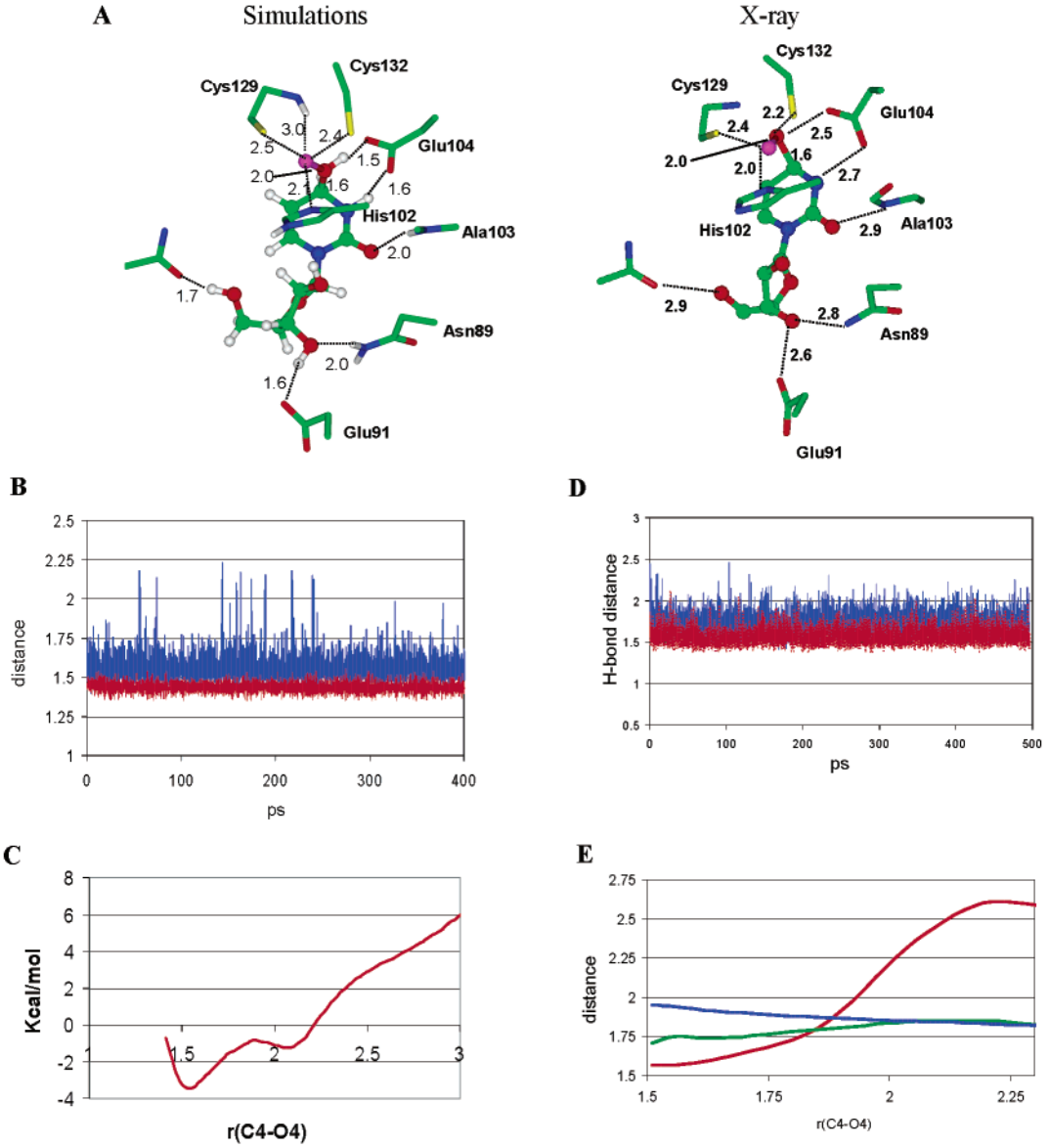

Figure 2. (A) (Left) average active-site structure obtained from 2000 frames (or 100 ps) of the molecular dynamics simulations of the CDA−ZEB−H_2O complex. The further increase of the number of frames has little effect on the structure. Distances are in ångstroms. The 4-OH group of ZEB−H_2O is coordinated to the zinc ion (2.0 Å) and hydrogen bonded to OE1 of Glu104 (1.5 Å). The C_4−O_4 bond has an average distance of about 1.6 Å. OE_2 of Glu-104 receives a hydrogen bond from the 3-NH group (1.6 Å). The additional ligands to zinc include Cys-129, Cys-132, and His-102. Glu-91 and Asn-89 interact with the 3′-OH group. (Right) X-ray structure from ref 11. (B) The motion of ZEB−H_2O in the active site of CDA as a function of time monitored by the C_4−O_4 distance (blue) and C_3'−O_3' distance (red). The distance fluctuations of the C_4−O_4 bond are significantly larger than those of the C_3'−O_3' bond. Also, the C_4−O_4 bond undergoes transient bond-breaking and -making on a picoseconds scale during the simulations; the bond distance approaches or exceeds 2.0 Å about 2−3% of the time. (C) Free energy (potential of mean force) as a function of the C_4−O_4 distance. There is a second minimum near $r(C_4$−$O_4) = 2$ Å, corresponding to the transient structures with the relatively long C_4−O_4 distances observed in Figure 2A. The free energy difference of the two minima is about 2.5 kcal/mol; the structure with the shorter C4−O4 distance is more stable in the wild-type enzyme. (D) Fluctuations of the OE_1 (Glu-104)···H (O_4) (red) and OE_2 (Glu-104)···H_3 (N_3) (blue) hydrogen bond distances as functions of time. The average distance for the OE_1···H(O_4) hydrogen bond (1.6 Å) is shorter than that for the OE_2···H_3(N_3) hydrogen bond (1.75 Å), suggesting that the former is more stable. (E) Average distances for the OE_1···H (O_4) (red), OE_2···H_3 (N_3) (green), and Zn···O_4 (blue) interactions as functions of the C_4−O_4 distance. These average distances are obtained from the trajectories of the umbrella sampling, and the corresponding free energy information is given in Figure 2C (see Methods). The distance that undergoes the most significant change is the OE_1···H (O_4) hydrogen bond. This hydrogen bond is rather strong (based on the hydrogen bond distance) when the C4−O4 covalent bond is intact, but rather weak when the C_4−O_4 bond is broken. The distance between O_4 and Zn decreases (from 1.95 to 1.81 Å) with increasing the C_4−O_4 distance (from 1.5 to 2.3 Å).

nation on the nucleophilic attack by the zinc hydroxide, the simulations were performed on the complex where the proton was placed on OE_2 rather than 3-N. It was found that the C_4−O_4 bond was broken during the energy minimization, leading to ZEB and the zinc hydroxide group. The zinc hydroxide group was unable to approach C_4 with a distance of less than 2 Å during the MD simulations (data not shown); the average C_4−O_4 distance is 2.2 Å. Thus, the results of the simulations suggest that the protonation of 3-N would make the nucleophilic attack much easier.

ZEB−H_2O in E104A. To obtain additional information concerning the role of Glu104 in stabilizing ZEB−H_2O, Glu-104 was replaced by Ala. Figure 3A plots the active site structures representing three different stages observed during the MD simulations; only the interactions involving the pyrimidine ring are shown. The structure on the left represents the

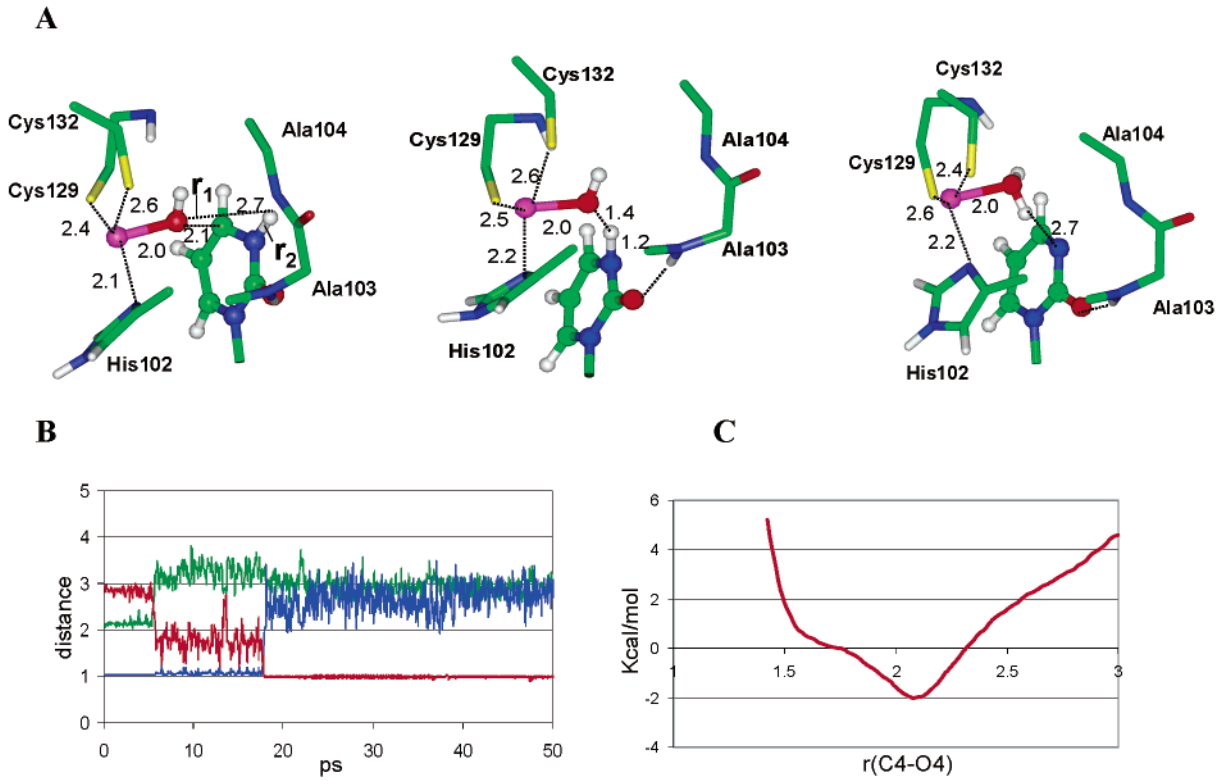

Figure 3. (A) Dehydration of ZEB−H_2O into ZEB and a water molecule observed during the QM/MM MD simulations of the E104A-ZEB−H_2O complex. (Left) early stage of the simulations. The 4-OH group exists as the zinc hydroxide ion and is on the top of C_4 with a C_4−O_4 distance of about 2.5−3.0 Å. (Middle) next stage of the dehydration. The zinc activated hydroxide oxygen interacts with the 3-NH group and shares the proton with N_3. (Right) final stage of the dehydration. The hydroxide ion has picked up the proton from N_3 and changed to water. It moved back to the initial position on the top of C_4. The umbrella sampling simulations were performed using the difference between $r_1(O_4\cdots H_3)$ and $r_2(N_3-H_3)$ (see Figure 3A) as the reaction coordinate (i.e., $r_1 - r_2$). The free energy decreases by about 20 kcal/mol as the proton transfers from 3-N to the hydroxide ion. (B) Dehydration of ZEB−H_2O monitored by the O_4−H_3 (red), N_3−H_3 (blue), and C_4−O_4 (green) distances. The O_4−H_3 distance changes from a distance of 3 to 1.5 Å (i.e., corresponding to the change from the structure on the left to the one in the middle in Figure 3A). It then changes to 1 Å (i.e., corresponding to the change to the structure on the right in Figure 3A), and at the same time the N_3−H_3 bond is broken with the corresponding distance increases to about 3 Å. (C) Free energy (potential of mean force) as a function of the C_4−O_4 distance in the E104A mutant. The mutation of Glu-104 to Ala shifted the minimum of the free energy curve along the C_4−O_4 bond to the other location at $r(C_4-O_4) \sim 2.2$ Å identified earlier (Figure 2C).

early stage of the simulations. As can be seen from this structure, the C_4−O_4 bond is broken and the 4-OH group exists as a zinc hydroxide ion. The figure in the middle shows the active structure observed in the next stage of the simulations. The zinc activated hydroxide oxygen has moved significantly and is now in the position to interact with the 3-NH group. The figure on the right shows the active site structure in the final stage; this structure was found to be stable during the rest of the simulations. As can be seen from this figure, the hydroxide ion has already picked up the proton from N_3 and moved back to the initial position (i.e., on the top of C_4), leading to the dehydration of ZEB−H_2O into zebularine and a water molecule. The umbrella sampling method was used to determine the free energy change associated with the process given in Figure 3A. It was found that the free energy decreases by about 20 kcal/mol as the proton transfers from 3-N to the hydroxide ion. Thus, the results of the simulations suggest that the hydroxide ion is unstable without the presence of Glu-104. In Figure 3B, the O_4−H_3, N_3−H_3, and C_4−O_4 distances are used to monitor the process shown in Figure 3A. As can be seen from Figure 3B, the O_4−H_3 distance (red line) first changes from a distance of 3 to 1.5 Å so that O_4 can interact with 3-NH. It then changes to 1 Å, indicating that the covalent bond is formed between O_4 and H_3. At the same time the N_3−H_3 bond (blue line) is broken.

Figure 3C shows the free energy (potential of mean force) as a function of the C_4−O_4 distance in the E104A mutant (i.e., before the proton transfer discussed earlier); the free energy curve was obtained in the same way as the one given in Figure 2C except that Glu104 was replaced by Ala. Consistent with the earlier observation, the C_4−O_4 bond becomes unstable and cannot be formed in the mutant. It is interesting to note from Figure 3C that the mutation of Glu-104 to Ala shifted the minimum on the free energy curve to the other location at $r(C_4-O_4) \sim 2.1$ Å identified earlier in the wild-type enzyme.

Discussions

One of the key events in the CDA-catalyzed reaction is the nucleophilic attack by the zinc hydroxide group on C_4, leading to the formation of the hypothetical tetrahedral intermediate (Figure 1A). Thus, an important question is how CDA would be able to stabilize this intermediate state and to lower the energy barrier for the reaction. The ability of zebularine 3,4-hydrate (ZEB−H_2O) to mimic the intermediate structure and to capture a fraction of the affinity for the transition state implies that the forces responsible for the structural stability and integrity of ZEB−H_2O in the active site may also be responsible for the transition state stabilization. Thus, understanding how the enzyme is able to stabilize this rare 3,4-hydrated species in the active site may provide important insights into the mechanism of the CDA-catalyzed reaction. The results of the QM/MM MD simulations reported here demonstrate that ZEB−H_2O is generally stable in the active site of the wild-type enzyme with an

average structure close to the one observed experimentally (Figure 2A). However, its C_4-O_4 bond undergoes transient bond-breaking and -making (Figure 2B); the bond-making process resembles the nucleophilic attack by the hydroxide group on C_4 of ZEB in the hydration process. Thus, the dynamic behavior of the C_4-O_4 bond seems to be quite different from that of conventional covalent bonds (compare, for example, the fluctuations of the C_4-O_4 and $C_3'-O_3'$ bonds in Figure 2B). It would be of interest to confirm this prediction experimentally and examine if this interesting dynamic behavior exists in other enzyme−TSA complexes. The observation from the X-ray crystallography[11] that this bond is unusually long in the TSA complex is consistent with the simulation results (see above). But it does not provide a direct support for the dynamic behavior. The umbrella sampling simulations showed that there is equilibrium between two different types of the structures in the active site with different C_4-O_4 distances (Figure 2C). These two types of the structures correspond to the stages before and after the nucleophilic attack, respectively.

The question is how the active site interactions are able to shift the equilibrium and lead to the formation of zebularine 3,4-hydrate and, presumably, the stabilization of the tetrahedral intermediate as well during the catalysis. Examination of the interactions as functions of the C_4-O_4 distance revealed that the interaction that undergoes the most significant change during the formation of the C_4-O_4 bond is the hydrogen bond between OE_1(Glu-104) and $H(O_4)$ (see Figure 2E). In particular, OE_1 and the 4-OH group can form a strong hydrogen bond only when the C_4-O_4 distance is short (l.5−1.7 Å). The corresponding differential hydrogen bonding energy should be able to make an important contribution to the stability of ZEB−H_2O in the active site and, presumably, to transition state stabilization as well. The role of the OE_1 (Glu-104)···$H(O_4)$ hydrogen bond in transition state stabilization has been a subject of previous discussions. It was shown that the hydrogen bond distance for this interaction in the CDA−ZEB complex is 0.2 Å shorter than the corresponding distance in the CDA−DHZ complex (i.e., between OE_1 and a trapped water). This observation has led to the suggestion that the strength of this hydrogen bond may increase with the development of the C_4-O_4 covalent character and the energetic effect would be used for the transition state stabilization. The results of this study support this previous suggestion and provide a direct computational evidence that the nucleophilic attack by the zinc hydroxide group on C_4 leads to the strengthening of the OE_1(Glu-104)···$H(O_4)$ hydrogen bond.

It was suggested that one of the reasons for the increase of the strength of the OE_1(Glu-104)···$H(O_4)$ hydrogen bond is that the formation of the C_4-O_4 bond converts the zinc-bound oxygen into a species more closely resembling an alkoxide group than a hydroxyl group. As a result, the pK_a of the 4-OH proton would be depressed toward that of the carboxylate, leading to a stronger interaction between these two groups. Other factors may be involved as well. For instance, the formation of the C_4-O_4 bond leads to smaller fluctuations for the OH group, making its interaction with OE_1 more stable. Moreover, the 3-NH and 4-OH groups of ZEB−H_2O (i.e., with an unbroken C_4-O_4 bond) seem to be in ideal relative positions to match OE_1 and OE_2 of the carboxylate group from Glu-104 (see Figure 2A). The simultaneous formations of these two strong hydrogen bonds may help to hold the two fragments of ZEB−H_2O together and prevent the C_4-O_4 bond from being broken.

The results discussed above indicate that the interactions involving Glu-104 are essential for stabilizing ZEB−H_2O in the active site of the wild-type enzyme. The QM/MM MD simulations on the E104A-ZEB−H_2O complex provide additional insights concerning the role of Glu-104. It was shown that when Glu-104 was replaced by Ala, the covalent bond between C_4 and the 4-OH group in ZEB−H_2O was broken followed by a proton transfer from the 3-NH group to the hydroxide, leading to the dehydration of ZEB−H_2O into ZEB and a water molecule (Figure 3A,B). Thus, ZEB− H_2O is likely to be rather unstable in the E104A mutant. It has been observed from ^{19}F NMR resonance[13] that whereas the wild-type enzyme binds FZEB (whose structure is very close to that of ZEB) as the 3,4-hydrated species (FZEB−H_2O), the E104A mutant binds the inhibitor without modification in a form that resembles the substrate in the ground state. Our results are therefore consistent with the experimental observations. Moreover, the simulations suggest that the active site water may not be in split form in E104A. This is in contrast with the case for the wild-type enzyme where the water is believed to be in split form with the hydroxide ion on zinc and proton on Glu-104.[19,20] This might contribute to the loss of the activity as a result of the mutation;[14] it could also be related to the different affinities of the wild-type enzyme and E104A mutant toward substrate cytidine.[13]

The results of the simulations demonstrated that understanding the stability and integrity of well-designed tight binding TSA's in the enzymes active sites may provide important insights into the origin of transition state stabilization during the catalysis.

Acknowledgment. This work was supported by a start-up fund from the Center of Excellence in Structural Biology, University of Tennessee. We are grateful for the computational resources from the Center for Computational Sciences, Oak Ridge National Laboratory, the National Center for Supercomputing Applications (NCSA), and the Scientific Computing Facilities of Boston University. We thank Prof. Martin Karplus for a gift of the CHARMM program and Prof. Qiang Cui for the help with the WHAM analysis.

References and Notes

(1) Wolfenden, R. *Nature* **1969**, *223*, 704−705.

(2) Wolfenden, R. *Acc. Chem. Res*. **1972**, *5*, 10−18.

(3) Wolfenden, R.; Kati, W. M. *Acc. Chem. Res.* **1991**, *24*, 209.

(4) Wolfenden, R. *Annu. Rev. Biophys. Bioeng*. **1976**, *5*, 271−306.

(5) Radzicka, A.; Wolfenden, R. *Methods Enzymol*. **1995**, *249*, 284.

(6) Schramm, V. L. *Annu. Rev. Biochem*. **1998**, *67*, 693−720.

(7) Morrison, J. F.; Walsh, C. T. *Adv. Enzymol. Relat. Area Mol. Biol.* **1988,** *61*, 201−301.

(8) Mader, M. M.; Bartlett, P. A. *Chem. Rev*. **1997**, *97*, 1281−1301.

(9) Lolis, E.; Petsko, G. A. *Annu. Rev. Biochem*. **1990**, *59*, 597−630.

(10) Lipscomb, WN.; Strater, N. *Chem. Rev.* **1996**, *96*, 2375−2433.

(11) Xiang, S.; Short, S. A.; Wolfenden, R.; Carter, C. W., Jr. *Biochemistry* **1995**, *34*, 4516−4523.

(12) Betts, L.; Xiang, S.; Short, S. A.; Wolfenden, R.; Carter, C. W., Jr. *J. Mol. Biol.* **1994**, *235*, 635−656.

(13) Carlow, D. C.; Short, S. A.; Wolfenden, R. *Biochemistry* **1996**, *35*, 5, 948−954.

(14) Carlow, D. C.; Smith, A. A.; Yang, C. C.; Short, S. A.; Wolfenden, R. *Biochemistry* **1995**, *34*, 4220−4224.

(15) Smith, A. A.; Carlow, D. C.; Wolfenden, R.; Short, S. A. *Biochemistry* **1994**, *33*, 6468−6474.

(16) Snider, M. J.; Gaunitz, S.; Ridgway, C.; Short, S. A.; Wolfenden, R. *Biochemistry* **2000**, *39*, 9746−9753.

(17) Xiang, S.; Short, S. A.; Wolfenden, R.; Carter, C. W., Jr. *Biochemistry* **1996**, *35*, 1335−1341.

(18) Xiang, S.; Short, S. A.; Wolfenden, R.; Carter, C. W., Jr. *Biochemistry* **1997**, *36*, 4768−4774.

(19) Snider, M. J.; Wolfenden, R. *Biochemistry* **2001**, *40*, 11364−11371.
(20) Lewis, J. P.; Carter, C. W., Jr.; Hermans, J.; Pan, W.; Lee, T.-S.; Yang, W. *J. Am. Chem. Soc*. **1998**, *120*, 5407−5410.
(21) Lewis, J. P.; Liu, S.; Lee, T.-S.; Yang, W. 1999 *J. Comput. Phys*. **1999**, *151*, 242-263.
(22) Frick, L.; MacNeela, J. P.; Wolfenden, R. *Bioorg. Chem*. **1987**, *15*, 100−108.
(23) Frick, L.; Yang, C.; Marquez, V. E.; Wolfenden, R. *Biochemistry* **1989**, *28*, 9423−9430.
(24) Snider, MJ.; Reinhardt, L.; Wolfenden, R.; Cleland, WW. *Biochemistry* **2002**, *41*, 415−421.
(25) (a) Cui, Q.; Elstner, M.; Kaxiras, E.; Frauenheim, T.; Karplus, M. *J. Phys. Chem*. **2001**, *B 105*, 569−585. (b) Elstner, M.; Cui, Q.; Munih, P.; Kaxiras, E.; Frauenheim, T.; Karplus, M. *J. Comput. Chem*. **2003**, *24*, 565−581.
(26) For a recent review of the QM/MM methods and the summary of the applications, see: Gao, J.; Truhlar, D. G. *Annu. Rev. Phys. Chem*. **2002**, *53*, 467−505.
(27) Brooks, B. R.; Bruccoleri, R. E.; Olafson, B. D.; States, D. J.; Swaminathan, S.; Karplus, M. *J. Comput. Chem.* **1983**, *4*, 187−217.
(28) Guo, H.; Cui, Q.; Lipscomb, W. L.; Karplus, M. *Proc. Natl. Acad. Sci. U.S.A.* **2001**, *98*, 9032−9037.
(29) Guo, H.; Cui, Q.; Lipscomb, W. L.; Karplus, M. *Angew. Chem., Int. Ed.* **2003**, *42*, 1508−1511.
(30) MacKerell, A. D., Jr.; Bashford, D.; Bellott, M.; Dunbrack, R. L., Jr.; Evanseck, J. D.; Field, M. J.; Fischer, S.; Gao, J.; Guo, H.; Ha, S.; et al. *J. Phys. Chem. B* **1998**, *102*, 3586−3616.
(31) Jorgensen, W. L. *J. Am. Chem. Soc*. **1981**, *103*, 335−340.
(32) Neria, E.; Fisher, S.; Karplus, M. *J. Chem. Phys*. **1996**, *105*, 1902−1921.
(33) Brooks, C. L., III; Brunger, A.; Karplus, M. *Biopolymers* **1985**, *24*, 843−865.
(34) Torrie, G. M.; Valleau, J. P. *Chem. Phys. Lett*. **1974**, *28*, 578.
(35) Kumar, M.; Bouzida, D.; Swendsen, R. H.; Kollman, P. A.; Rosenberg, J. M. *J. Comput. Chem*. **1992,** *13*, 1011−1021.